

Importance of long-ranged electron-electron interactions for the magnetic phase diagram of twisted bilayer graphene

Lennart Klebl,¹ Zachary A. H. Goodwin,² Arash A. Mostofi,² Dante M. Kennes,^{1,3} and Johannes Lischner²

¹*Institute for Theory of Statistical Physics, RWTH Aachen University,
and JARA Fundamentals of Future Information Technology, 52062 Aachen, Germany*

²*Departments of Materials and Physics and the Thomas Young Centre for Theory and Simulation of Materials,
Imperial College London, South Kensington Campus, London SW7 2AZ, UK*

³*Max Planck Institute for the Structure and Dynamics of Matter,
Center for Free Electron Laser Science, 22761 Hamburg, Germany*

(Dated: May 6, 2022)

Electron-electron interactions are intrinsically long ranged, but many models of strongly interacting electrons only take short-ranged interactions into account. Here, we present results of atomistic calculations including both long-ranged and short-ranged electron-electron interactions for the magnetic phase diagram of twisted bilayer graphene and demonstrate that qualitatively different results are obtained when long-ranged interactions are neglected. In particular, we use Hartree theory augmented with Hubbard interactions and calculate the interacting spin susceptibility at a range of doping levels and twist angles near the magic angle to identify the dominant magnetic instabilities. At the magic angle, mostly anti-ferromagnetic order is found, while ferromagnetism dominates at other twist angles. Moreover, long-ranged interactions significantly increase the twist angle window in which strong correlation phenomena can be expected. These findings are in good agreement with available experimental data.

INTRODUCTION

Since the discovery of superconductivity in proximity to correlated insulator states at half (electron or hole) filling of the flat bands [1, 2], there has been great interest in the electronic properties of magic-angle twisted bilayer graphene (tBLG) [3]. Additional experiments [4–10] discovered correlated insulator phases and superconductivity at other doping levels of the flat bands and revealed a wide range of interesting phenomena [11, 12] including strange metal behaviour [13, 14], ferromagnetic order [15, 16], superconductivity without correlated insulators [17–19], Chern insulators [20–22], and nematic states [6, 23–25].

These findings demonstrate the importance of electron-electron interactions for understanding the electronic properties of tBLG [11, 12]. The quintessential model for strongly interacting electrons is the Hubbard model, in which electrons only interact when they are on the same “site” (typically assumed to be an atom). In tBLG near the magic angle, the moiré pattern results in the emergence of eight flat bands (including a factor of two from spin degeneracy) near the Fermi energy which are separated from all other bands by energy gaps [26–34]. Starting from atomistic tight-binding approaches, Hubbard models for tBLG can be obtained by constructing Wannier functions of the flat bands [35–37] (note that this is not possible when a continuum model starting point is used; in that case additional bands must be included in the Wannierization procedure [38, 39]). The properties of such models have been studied using mean-field theory, the functional renormalization group [40, 41] and exact diagonalization [10] resulting in many important insights

into the origin of superconductivity and correlated insulator states. Instead of using flat-band Wannier functions which are extended over the whole moiré unit cell as a basis, it is also possible to construct atomistic Hubbard models using a basis of carbon p_z orbitals [42–44].

Importantly, Hubbard models only capture short-ranged electron-electron interactions [45]. It is well known, however, that long-ranged interactions play an important role in tBLG. Using Hartree theory, several groups [46–50] demonstrated that long-ranged interactions result in significant changes of the electronic structure which depend sensitively on doping and twist angle. In particular, Hartree interactions result in a flattening of the doped bands (in addition to the band flattening induced by twisting) [26–29]. This interaction-induced band flattening explains the Fermi level pinning that was observed in several recent scanning tunnelling spectroscopy measurements [10, 23].

Therefore, accurate models of tBLG should capture both short-ranged and long-ranged electron-electron interactions. To achieve this, several groups used Hartree-Fock calculations based on a continuum model of the electronic structure [51–55]. While these calculations have yielded many useful insights, they do not capture atomic-scale interactions (such as onsite interactions within carbon p_z -orbitals) and often only include a few bands near the Fermi level with the effect of all other bands being described by an effective dielectric constant. Few groups have attempted to capture the interplay of long-ranged and short-ranged interactions using atomistic calculations: González and Stauber [56] studied the properties of tBLG in different dielectric environments using atomistic Hartree-Fock theory, and Sboychakov *et al.* [57]

developed an atomistic Hubbard model with long-ranged electron-electron interactions. These studies investigated the properties of tBLG at a single twist angle focusing on the undoped system and did not study in detail the doping dependence and twist-angle dependence of the interplay of long-ranged and short-range interactions.

In this paper, we calculate the magnetic phase diagram of tBLG as function of twist angle and doping using an atomistic Hartree theory with additional Hubbard interactions. Specifically, we calculate the interacting spin susceptibility and determine the critical value of the Hubbard U parameter that is required to induce a magnetic instability. Our calculations predict magnetic instabilities over a relatively large twist angle window ranging from 0.96° to 1.16° . Near the magic angle, the magnetic ordering is mostly anti-ferromagnetic, while at other twist angles ferromagnetism dominates. When Hartree interactions are neglected, a qualitatively different phase diagram with a much smaller critical twist angle window is found. Finally, we compare our findings with available experimental data and overall find good agreement.

METHODS

We study commensurate unit cells of tBLG with D_3 symmetry [28, 29]. The atomic positions are relaxed using classical force-fields [30–34]. For this, we use a combination of the AIREBO-Morse [58] and Kolmogorov–Crespi [59] potentials as implemented in LAMMPS [60].

To investigate magnetic ordering tendencies of tBLG including the effect of long-ranged interactions, we calculate the interacting static spin susceptibility in the normal state using a Hartree theory plus U (Hartree+ U) approach. In this approach, Hubbard interactions within the carbon p_z -orbitals are captured by adding a Hubbard contribution $U \sum_i n_{i\uparrow} n_{i\downarrow}$ (with U denoting the Hubbard parameter and $n_{i\uparrow}(n_{i\downarrow})$ denoting the occupancy of the up(down)-spin p_z -orbital on carbon atom i) to the Hartree theory total energy. The Hartree Hamiltonian is given by

$$\hat{H}_H = \sum_{ij} t(\boldsymbol{\tau}_i - \boldsymbol{\tau}_j) \hat{c}_i^\dagger \hat{c}_j + \sum_i V(\boldsymbol{\tau}_i) \hat{c}_i^\dagger \hat{c}_i, \quad (1)$$

where $\boldsymbol{\tau}_i$ is the position vector of carbon atom i and the corresponding annihilation (creation) operators are denoted by $\hat{c}_i^{(\dagger)}$. The hopping parameters $t(\mathbf{r})$ are determined using the Slater-Koster rules [28, 29, 61]. For this, we use the parameterization from Refs. 29 and 62:

$$t(\mathbf{r}) = t_\sigma e^{q_\sigma(1-|\mathbf{r}|/d)} \cos^2 \varphi + t_\pi e^{q_\pi(1-|\mathbf{r}|/a)} \sin^2 \varphi, \quad (2)$$

where $t_\sigma = 0.48$ eV and $t_\pi = -2.7$ eV are, respectively, the sigma and pi hopping between carbon p_z orbitals, and

$d = 3.3$ Å and $a = 1.4$ Å denote the interlayer separation and carbon-carbon bond length, respectively. Also, $q_\sigma = d/(0.184a)$ and $q_\pi = 1/0.184$ are decay parameters and φ is the inclination angle of the orbitals.

The second term in Eq. (1) describes long-ranged Hartree interactions with $V(\boldsymbol{\tau}_i)$ denoting the Hartree potential at position $\boldsymbol{\tau}_i$. The Hartree potential is given by

$$V(\boldsymbol{\tau}_i) = \sum_j (n_j - \bar{n}) W_{ij}, \quad (3)$$

where n_j denotes the occupancy of the p_z orbital on atom j and \bar{n} is the average occupancy. Also, W_{ij} denotes the screened Coulomb interaction between electrons at $\boldsymbol{\tau}_i$ and $\boldsymbol{\tau}_j$ [49]. In principle, $V(\boldsymbol{\tau}_i)$ must be determined self-consistently, but it has been shown [46, 47, 49] that the resulting potential is accurately described by

$$V(\boldsymbol{\tau}_i) = (\nu - \nu_0) V_0 \sum_{j=1,2,3} \cos(\mathbf{b}_j \cdot \boldsymbol{\tau}_i), \quad (4)$$

where ν is the number of added electrons per moiré unit cell (relative to charge neutrality) and \mathbf{b}_j denote the three shortest reciprocal lattice vectors of the moiré unit cell. We use $V_0 = 5$ meV and $\nu_0 = 0$ [49]. These parameters include internal screening from tBLG [63, 64]. Additional screening from the substrate or metallic gates [49, 50, 65] results in a further reduction of V_0 . Note that Eq. (4) assumes that the AA regions reside in the corners of the rhombus-shaped moiré unit cell.

Within the Hartree+ U approach, the frequency- and wavevector-dependent interacting spin susceptibility $\chi_{ij}(\mathbf{q}, q_0)$ (with i and j denoting carbon p_z -orbitals and \mathbf{q} and q_0 being a wavevector and frequency, respectively) is given by [43]

$$\hat{\chi}(\mathbf{q}, q_0) = \hat{\chi}^{(0)}(\mathbf{q}, q_0) [\mathbb{1} + U \hat{\chi}^{(0)}(\mathbf{q}, q_0)]^{-1}. \quad (5)$$

Here, $\hat{\chi}^{(0)}$ denotes the non-interacting spin-response function

$$\chi_{ij}^{(0)}(\mathbf{q}, q_0) = \frac{1}{N_{\mathbf{k}} \beta} \sum_{\mathbf{k}, k_0} G_{ij}(\mathbf{k}, k_0) G_{ji}(\mathbf{k} + \mathbf{q}, k_0 + q_0), \quad (6)$$

where $\hat{G}(\mathbf{k}, k_0) = (ik_0 - \hat{\mathcal{H}}_H(\mathbf{k}) + \mu)^{-1}$ is the Matsubara Green's function of the Hartree Hamiltonian for states with crystal momentum \mathbf{k} . Also, μ denotes the chemical potential, $N_{\mathbf{k}}$ is the number of momentum points used to sample the first Brillouin zone ($N_{\mathbf{k}} = 24$) and $\beta = 1/(k_B T)$ (with k_B and T denoting the Boltzmann constant and temperature, respectively). The Matsubara (k_0) summation is carried out numerically using an appropriately chosen grid with $N_\omega = 500$ frequencies – this reduces the computational effort compared to the analytical evaluation [43]. For comparison, we also calculate the interacting spin susceptibility without long-ranged interactions, i.e., setting $V(\boldsymbol{\tau}_i) = 0$.

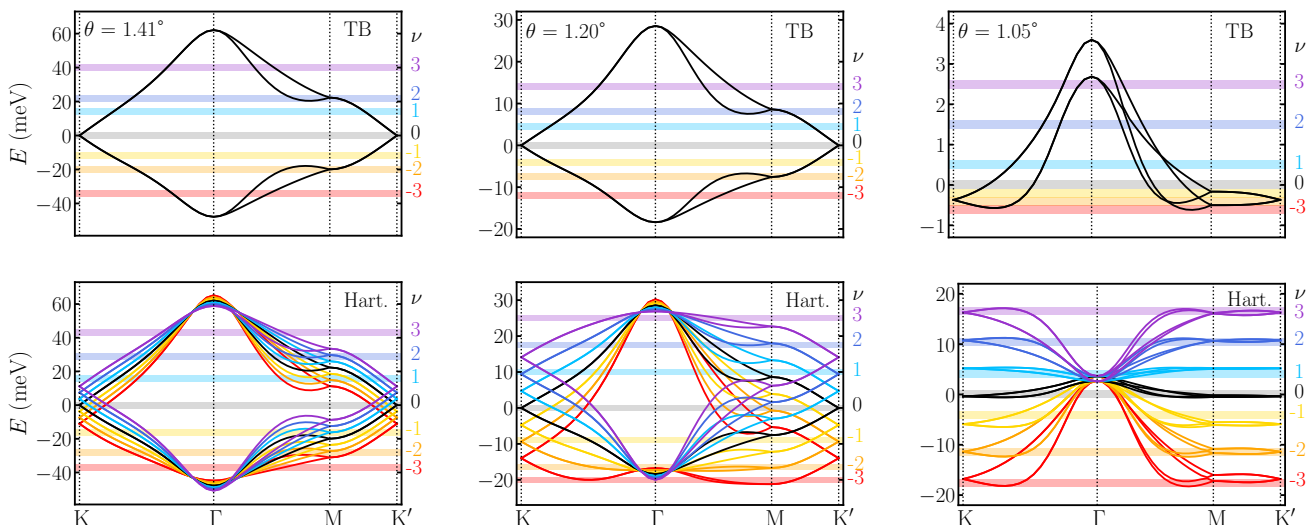


FIG. 1. Band structures of tBLG at twist angles of 1.41° , 1.20° and 1.05° for various integer fillings ν of the flat bands from tight-binding (denoted TB, see upper panels) and Hartree theory (denoted Hart., see lower panels). Fermi levels are indicated by horizontal lines. In contrast to Hartree theory, the tight-binding band structure does not depend on ν . Note that the energy scale on the y -axis is different in each panel. The zero of energy for each plot is taken to be the Dirac point energy from tight-binding.

We focus on low-temperature static instabilities that maintain the translational symmetry of the moiré lattice and therefore use $\beta = 10^4 \text{ eV}^{-1}$ and $\mathbf{q} = \mathbf{q}_0 = 0$. Magnetic instabilities occur when an eigenvalue of χ_{ij} diverges. The critical interaction strength that is required to induce the ordering is given by $U_c = -1/\lambda_0$, where λ_0 denotes the largest eigenvalue of $\chi_{ij}^{(0)}$. This is a generalization of the well-known Stoner criterion of ferromagnetism [66]. The corresponding eigenvector v_i of χ_{ij} characterizes the spatial structure of the resulting magnetic order.

RESULTS

Figure 1 shows the band structures from Hartree theory at three twist angles near the magic angle ($\theta = 1.41^\circ$, 1.20° and 1.05°) at various doping levels. For comparison, we also show the corresponding tight-binding results. For the two larger twist angles, both the Hartree and tight-binding band structures exhibit Dirac cones at the K and K' points. While the non-interacting tight-binding band structure does not depend on the doping level, long-ranged electron-electron interactions captured by Hartree theory give rise to a significant doping-dependent distortion of the band structure [46–50]. In particular, Hartree interactions result in a flattening of the doped bands. For example, at $\theta = 1.20^\circ$ and $\nu = 3$ the two higher-energy bands are much flatter than the corresponding tight-binding bands.

The magic angle (defined as the twist angle with the smallest width of the flat band manifold) is found to be

1.05° . At this twist angle, the tight-binding band structure differs qualitatively from the result at larger (and smaller) twist angles. In particular, the lower-energy bands are inverted and have a similar shape to the higher-energy bands. Including long-ranged interactions again results in drastic changes to the band structure with Hartree theory predicting an increase of the overall flat band width when the system is doped. Also, the overall shape of the flat band manifold is flipped when comparing hole-doped and electron-doped systems. For more detailed discussions of the Hartree-theory band structures, we refer the interested reader to Refs. 46–50.

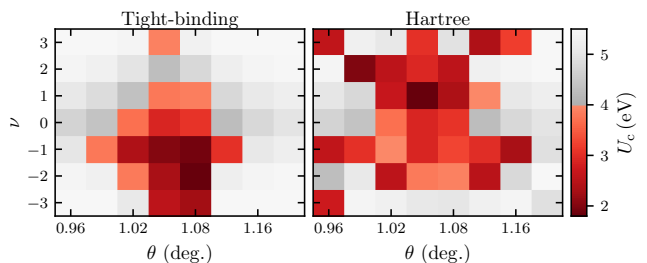


FIG. 2. Critical Hubbard interaction strength U_c required for the onset of magnetic instabilities as a function of flat band filling ν and twist angle θ . Left panel: without Hartree interactions (tight-binding). Right panel: with Hartree interactions.

Next, we calculate the interacting spin susceptibility from Hartree+ U theory as function of doping at a wide range of twist angles near the magic angle (0.96° , 0.99° , 1.02° , 1.05° , 1.08° , 1.12° , 1.16° and 1.20°). Fig. 2 compares the critical Hubbard parameter U_c without Hartree

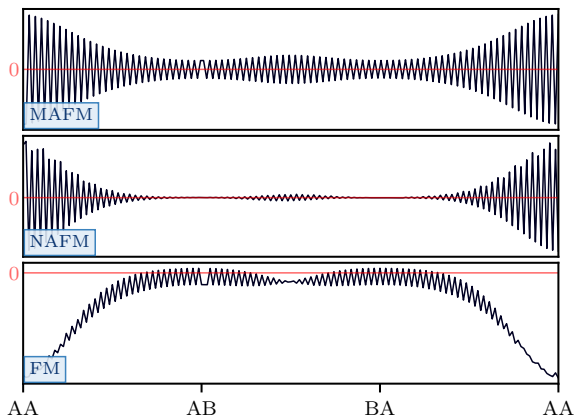


FIG. 3. Dominant magnetic orderings in twisted bilayer graphene near the magic angle. Shown is a linecut of the magnetic order parameter (spin density) along the diagonal of the rhombus-shaped moiré unit cell. Top panel: Ångström scale anti-ferromagnetic with a modulation on the moiré scale (MAFM). Middle panel: Ångström scale anti-ferromagnetic with nodes in the AB and BA regions (NAFM). Bottom panel: mostly ferromagnetic (FM) order.

interactions (left panel) and with Hartree interactions (right panel) as function of twist angle and doping. To assess if the system undergoes a phase transition, U_c must be compared with the actual value of U for a carbon p_z -orbital. In graphene, Wehling *et al.* [67] and Schuler *et al.* [68] found that $U \approx 4$ eV. We expect that screening from tBLG does not significantly alter this value, as the flat bands mainly screen long-ranged interactions [63, 64]. Therefore, we assume a doping and twist angle independent value of $U \approx 4$ eV in the following analysis.

Without Hartree interactions (left panel of Fig. 2), magnetic instabilities are found at twist angles ranging from 0.99° to 1.12° . At the magic angle ($\theta = 1.05^\circ$), instabilities occur at all integer doping levels except $\nu = 2$. At twist angles smaller or larger than the magic angle, instabilities are observed at a smaller set of doping levels. In particular, for $\theta = 0.99^\circ$ and $\theta = 1.12^\circ$, they only occur at $\nu = -1$. In general, the critical Hubbard parameters are smaller for hole doped systems because the lower-energy flat bands are somewhat flatter than the higher-energy ones in tight binding. For twist angles larger than 1.2° , we find $U_c \approx 5.5$ eV, which is similar to the value predicted for untwisted bilayer graphene [43].

When Hartree interactions are included (right panel of Fig. 2), a qualitatively different behaviour of U_c is observed near the magic angle. In particular, the lowest values of U_c are now found for electron-doped systems. Very close to the magic angle, U_c is lowest for $\nu = 1$. At twist angles somewhat smaller or larger than the magic angle, the lowest value of U_c is at $\nu = 2$ and at $\theta = 0.96^\circ$ or 1.16° the minimum is at $\nu = 3$. These findings can be understood from the Hartree theory band structures, Fig. 1, which show that the doping level which gives rise

to the flattest bands depends on the twist angle: at the magic angle the flattest bands are found at $\nu = \pm 1$, while at $\theta = 1.20^\circ$ the higher-energy bands are extremely flat at $\nu = \pm 3$.

Figure 2 also shows that magnetic instabilities occur over a larger twist angle range when long-ranged Hartree interactions are included. Specifically, the Hartree+ U approach predicts such instabilities for a twist-angle window from $\theta = 0.96^\circ$ to $\theta = 1.16^\circ$. This larger critical twist angle window is consistent with experimental findings: recent transport and tunnelling experiments reported correlated phases in a twist angle range from 1.0° to 1.2° [6, 11].

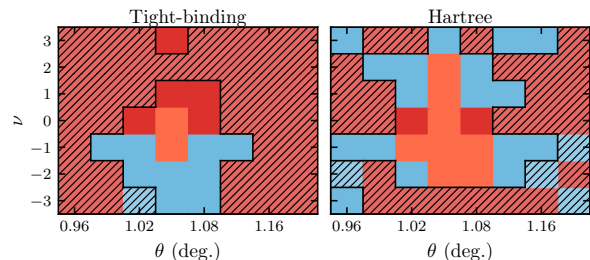


FIG. 4. Magnetic phase diagram of twisted bilayer graphene as function of flat band filling ν and twist angle θ : blue denotes ferromagnetic order, while red and orange indicate modulated anti-ferromagnetic order and nodal anti-ferromagnetic order, respectively. Left panel: without Hartree interactions (tight-binding). Right panel: with Hartree interactions. Note that magnetic phases with $U_c > 4$ eV are experimentally not relevant (hatched regions).

Next, we analyze the spatial structure of the magnetic phases: the leading magnetic instabilities are either Ångström scale anti-ferromagnetic with a modulation on the moiré scale (MAFM), Ångström scale anti-ferromagnetic with nodes in the AB and BA regions (NAFM) or mostly ferromagnetic (FM), see Fig. 3. Figure 4 shows the magnetic phase diagram as function of twist angle and doping near the magic angle. Without Hartree interactions, the hole doped system is typically ferromagnetic (except at the magic angle). Ferromagnetism is found to coincide with small values of U_c . In contrast, the undoped and electron doped system always exhibits modulated anti-ferromagnetic order (MAFM) with NAFM only occurring at $\nu = 0$ and $\nu = 1$ at the magic angle.

Dramatic qualitative changes in the magnetic phase diagram are observed when Hartree interactions are included, see right panel of Fig. 3. The region of NAFM order in $\nu - \theta$ -space is larger, while MAFM is only found for the undoped system at $\theta = 1.02^\circ$ and $\theta = 1.08^\circ$. Everywhere else the ordering is ferromagnetic. Again, occurrence of FM is correlated with low values of U_c which in turn are caused by flat bands induced by long-ranged Hartree interactions.

DISCUSSION

In this section, we compare our calculated magnetic phase diagram to experimental findings. Many experimental techniques, including transport and tunnelling measurements, probe quasiparticle properties of tBLG. While our analysis does not directly yield such properties, we use the value of the critical Hubbard parameter U_c as a proxy for the quasiparticle gap in the correlated insulator phases with small values of U_c corresponding to large gaps associated with pronounced resistive peaks in transport experiments.

At charge neutrality, Hartree+ U theory predicts small values of U_c near the magic angle (note that this does not depend on the inclusion of Hartree interactions). Experimentally, the situation is not clear, however, with some experiments reporting semi-metallic behaviour near the magic angle [1, 2, 4], while others (for very similar twist angles) observe a strong insulating state [5]. These conflicting results could arise from different levels of strain in the samples: Liu *et al.* [53] demonstrated that a C_3 broken symmetry state that is stabilized by strain retains its semi-metallic character because of the topological properties of the electron structure of tBLG.

Next, we consider the effect of doping. While at $\nu = -1$ insulating states are not often observed in experiments, clear signatures of insulating states have been found at $\nu = +1$ [4, 8, 14, 20]. This is consistent with the Hartree+ U results which yield lower values of U_c for $\nu = +1$ than for $\nu = -1$. Note that the opposite result is obtained when long-ranged Hartree interactions are neglected.

Experiments typically observe the strongest insulating states at $\nu = \pm 2$ [1, 2, 4, 5]. Without Hartree interactions, our calculations predict no broken symmetry states at $\nu = +2$. In contrast, Hartree+ U theory predicts magnetic states for both $\nu = +2$ and $\nu = -2$. In two recent experiments [17, 19], a thin dielectric spacer layer that separates the tBLG from metallic gates was used to enhance the screening of the electron-electron interactions in tBLG. This results in significant changes to the electronic phase diagram with correlated insulator states being “screened out” for most twist angles and doping levels [65]. Interestingly, these experiments find the insulating state at $\nu = 2$ to be most robust. Naively, one might expect that this system should be described by the magnetic phase diagram obtained without long-ranged Hartree interactions. However, changes in external screening only result in weak changes to the Hartree theory band structure [47, 49] and therefore we expect that the Hartree+ U result should be more relevant to experiments with thin dielectric spacer layers.

At $\nu = +3$, a strong insulating state is observed in experiments, especially when the tBLG is aligned with the hexagonal boron nitride substrate [15, 16]. In

contrast, the $\nu = -3$ insulating state is almost never seen [1, 4, 5, 20]. For insulating phases to emerge at these doping levels both valley and spin symmetries must be broken, i.e., the insulating state must be ferromagnetic [15, 16]. This is consistent with the Hartree+ U results which predict FM order at $\nu = +3$ at several twist angles near the magic angle. FM order at $\nu = -3$ is only found at $\theta = 0.96^\circ$. Without Hartree interactions, our calculations do not predict FM order at $\nu = +3$ and instead find relatively strong FM states at $\nu = -3$.

Hartree+ U theory also predicts that insulating states at $\nu = +3$ should occur over a relatively large twist angle range, while those at $\nu = +1$ are only found very close to the magic angle. This finding also appears to be consistent with experiments. For example, Yankowitz and coworkers [4] observed an insulating state at $\nu = +3$ for a twist angle of 1.14° , but no insulating state was found at $\nu = +1$.

Finally, our Hartree+ U results for the magnetic phase diagram also have important implications for superconductivity in tBLG. First, band flattening induced by Hartree interactions enhances the density of states at the Fermi level and therefore increases the transition temperature irrespective of the nature of the superconducting glue. In addition, this mechanism also increases the range of twist angles where superconductivity can be observed. Note that superconductivity is typically observed in the vicinity of correlated insulator states at non-integer doping levels. Naively, one would expect that in this doping regime damped spin fluctuations from the magnetic parent state play an important role. However, Fischer and coworkers [69] recently demonstrated the possibility of pairing by anti-ferromagnetic spin fluctuations in the vicinity of a ferromagnetic phase. Future work will investigate the predictions of Hartree+ U theory at non-integer doping levels.

ACKNOWLEDGEMENTS

We are grateful for helpful discussions with V. Vitale, K. Atalar and Xia Liang. ZG was supported through a studentship in the Centre for Doctoral Training on Theory and Simulation of Materials at Imperial College London funded by the EPSRC (EP/L015579/1). We acknowledge funding from EPSRC grant EP/S025324/1 and the Thomas Young Centre under grant number TYC-101. We acknowledge the Imperial College London Research Computing Service (DOI:10.14469/hpc/2232) for the computational resources used in carrying out this work. The Deutsche Forschungsgemeinschaft (DFG, German Research Foundation) is acknowledged for support through RTG 1995, within the Priority Program SPP 2244 “2DMP” and under Germany’s Excellence Strategy-Cluster of Excellence Matter and Light for Quantum Computing (ML4Q) EXC2004/1 - 390534769. We ac-

knowledge support from the Max Planck-New York City Center for Non-Equilibrium Quantum Phenomena. Spin susceptibility calculations were performed with computing resources granted by RWTH Aachen University under projects rwth0496 and rwth0589.

-
- [1] Y. Cao, V. Fatemi, A. Demir, S. Fang, S. L. Tomarken, J. Y. Luo, J. D. Sanchez-Yamagishi, K. Watanabe, T. Taniguchi, E. Kaxiras, R. C. Ashoori, and P. Jarillo-Herrero, *Nature* **556**, 80 (2018).
- [2] Y. Cao, V. Fatemi, S. Fang, K. Watanabe, T. Taniguchi, E. Kaxiras, and P. Jarillo-Herrero, *Nature* **556**, 43 (2018).
- [3] S. Carr, D. Massatt, S. Fang, P. Cazeaux, M. Luskin, and E. Kaxiras, *Phys. Rev. B* **95**, 075420 (2017).
- [4] M. Yankowitz, S. Chen, H. Polshyn, Y. Zhang, K. Watanabe, T. Taniguchi, D. Graf, A. F. Young, and C. R. Dean, *Science* **363**, 1059 (2019).
- [5] X. Lu, P. Stepanov, W. Yang, M. Xie, M. A. Aamir, I. Das, C. Urgell, K. Watanabe, T. Taniguchi, G. Zhang, A. Bachtold, A. H. MacDonald, and D. K. Efetov, *Nature* **574**, 653–657 (2019).
- [6] Y. Cao, D. Rodan-Legrain, J. M. Park, F. N. Yuan, K. Watanabe, T. Taniguchi, R. M. Fernandes, L. Fu, and P. Jarillo-Herrero, Nematicity and competing orders in superconducting magic-angle graphene (2020), arXiv:2004.04148 [cond-mat.mes-hall].
- [7] U. Zondiner, A. Rozen, D. Rodan-Legrain, Y. Cao, R. Queiroz, T. Taniguchi, K. Watanabe, Y. Oreg, F. von Oppen, A. Stern, E. Berg, P. Jarillo-Herrero, and S. Ilani, *Nature* **582**, 203 (2020).
- [8] X. Liu, Z. Wang, K. Watanabe, T. Taniguchi, O. Vafek, and J. Li, arXiv:2003.11072 (2020).
- [9] D. Wong, K. P. Nuckolls, M. Oh, B. Lian, S. J. Yonglong Xie, K. Watanabe, T. Taniguchi, B. A. Bernevig, and A. Yazdani, *Nature* **582**, 198–202 (2020).
- [10] Y. Xie, B. Lian, B. Jäck, X. Liu, C.-L. Chiu, K. Watanabe, T. Taniguchi, B. A. Bernevig, and A. Yazdani, *Nature* **572**, 101 (2019).
- [11] L. Balents, C. R. Dean, D. K. Efetov, and A. F. Young, *Nat. Phys.*, doi.org/10.1038/s41567 (2020).
- [12] D. M. Kennes, M. Claassen, L. Xian, A. Georges, A. J. Millis, J. Hone, C. R. Dean, D. N. Basov, A. Pasupathy, and A. Rubio, *Nature Physics* in press (arXiv:2011.12638) (2020).
- [13] Y. Cao, D. Chowdhury, D. Rodan-Legrain, O. Rubies-Bigordà, K. Watanabe, T. Taniguchi, T. Senthil, and P. Jarillo-Herrero, *Phys. Rev. Lett.* **124**, 076801 (2020).
- [14] H. Polshyn, M. Yankowitz, S. Chen, Y. Zhang, K. Watanabe, T. Taniguchi, C. R. Dean, and A. F. Young, *Nat. Phys.* **15**, 1011 (2019).
- [15] A. L. Sharpe, E. J. Fox, A. W. Barnard, J. Finney, K. Watanabe, T. Taniguchi, M. A. Kastner, and D. Goldhaber-Gordon, *Science* **365**, 605–608 (2019).
- [16] M. Serlin, C. L. Tschirhart, H. Polshyn, Y. Zhang, J. Zhu, K. Watanabe, T. Taniguchi, L. Balents, and A. F. Young, *Science* **367**, 900–903 (2020).
- [17] Y. Saito, J. Ge, K. Watanabe, T. Taniguchi, and A. F. Young, *Nat. Phys.*, doi.org/10.1038/s41567 (2020).
- [18] H. S. Arora, R. Polski, Y. Zhang, A. Thomson, Y. Choi, H. Kim, Z. Lin, I. Z. Wilson, X. Xu, J.-H. Chu, K. Watanabe, T. Taniguchi, J. Alicea, and S. Nadj-Perge, *Nature* **583**, 379–384 (2020).
- [19] P. Stepanov, I. Das, X. Lu, A. Fahimniya, K. Watanabe, T. Taniguchi, F. H. L. Koppens, J. Lischner, L. Levitov, and D. K. Efetov, *Nature* **583**, 375–378 (2020).
- [20] I. Das, X. Lu, J. Herzog-Arbeitman, Z.-D. Song, K. Watanabe, T. Taniguchi, B. A. Bernevig, and D. K. Efetov, arXiv:2007.13390 (2020).
- [21] S. Wu, Z. Zhang, K. Watanabe, T. Taniguchi, and E. Y. Andrei, arXiv:2007.03735 (2020).
- [22] K. P. Nuckolls, M. Oh, D. Wong, B. Lian, K. Watanabe, T. Taniguchi, B. A. Bernevig, and A. Yazdani, arXiv:2007.03810 (2020).
- [23] A. Kerelsky, L. J. McGilly, D. M. Kennes, L. Xian, M. Yankowitz, S. Chen, K. Watanabe, T. Taniguchi, J. Hone, C. Dean, A. Rubio, and A. N. Pasupathy, *Nature* **572**, 95 (2019).
- [24] Y. Jiang, X. Lai, K. Watanabe, T. Taniguchi, K. Haule, J. Mao, and E. Y. Andrei, *Nature* **573**, 91 (2019).
- [25] Y. Choi, J. Kemmer, Y. Peng, A. Thomson, H. Arora, R. Polski, Y. Zhang, H. Ren, J. Alicea, G. Refael, F. von Oppen, K. Watanabe, T. Taniguchi, and S. Nadj-Perge, *Nat. Phys.* **15**, 1174 (2019).
- [26] J. M. B. L. dos Santos, N. M. R. Peres, and A. H. C. Neto, *Phys. Rev. Lett.* **99**, 256802 (2007).
- [27] R. Bistritzer and A. H. MacDonald, *PNAS* **108**, 12233 (2010).
- [28] G. T. de Laissardière, D. Mayou, and L. Magaud, *Nano Lett.* **10**, 804 (2010).
- [29] G. T. de Laissardière, D. Mayou, and L. Magaud, *Phys. Rev. B* **86**, 125413 (2012).
- [30] G. Cantele, D. Alfè, F. Conte, V. Cataudella, D. Ninno, and P. Lucignano, arXiv:2004.14323v1 (2020).
- [31] S. K. Jain, V. Juričić, and G. T. Barkema, *2D Mater.* **4**, 015018 (2017).
- [32] F. Gargiulo and O. V. Yazyev, *2D Mater.* **5**, 015019 (2018).
- [33] F. Guinea and N. R. Walet, *Phys. Rev. B* **99**, 205134 (2019).
- [34] S. Carr, S. Fang, Z. Zhu, and E. Kaxiras, *Phys. Rev. Research* **1**, 013001 (2019).
- [35] M. Koshino, N. F. Q. Yuan, T. Koretsune, M. Ochi, K. Kuroki, and L. Fu, *Phys. Rev. X* **8**, 031087 (2018).
- [36] J. Kang and O. Vafek, *Phys. Rev. X* **8**, 031088 (2018).
- [37] Z. A. H. Goodwin, F. Corsetti, A. A. Mostofi, and J. Lischner, *Phys. Rev. B* **100**, 121106(R) (2019).
- [38] H. C. Po, L. Zou, T. Senthil, and A. Vishwanath, *Phys. Rev. B* **99**, 195455 (2019).
- [39] S. Carr, S. Fang, H. C. Po, A. Vishwanath, and E. Kaxiras, *Phys. Rev. Research* **1**, 033072 (2019).
- [40] D. M. Kennes, J. Lischner, and C. Karrasch, *Phys. Rev. B* **98**, 241407(R) (2018).
- [41] L. Klebl, D. M. Kennes, and C. Honerkamp, *Phys. Rev. B* **102**, 085109 (2020).
- [42] L. A. Gonzalez-Arraga, J. L. Lado, F. Guinea, and P. San-Jose, *Phys. Rev. Lett.* **119**, 107201 (2017).
- [43] L. Klebl and C. Honerkamp, *Phys. Rev. B* **100**, 155145 (2019).
- [44] A. Ramires and J. L. Lado, *Phys. Rev. B* **99**, 245118 (2019).
- [45] Note that Hubbard models using a basis of flat-band Wannier functions account for some long-ranged interac-

- tions because of the large size of the Wannier orbitals [35–37].
- [46] F. Guinea and N. R. Walet, PNAS **115**, 13174–13179 (2018).
- [47] T. Cea, N. R. Walet, and F. Guinea, Phys. Rev. B **100**, 205113 (2019).
- [48] L. Rademaker, D. A. Abanin, and P. Mellado, Phys. Rev. B **100**, 205114 (2019).
- [49] Z. A. H. Goodwin, V. Vitale, X. Liang, A. A. Mostofi, and J. Lischner, Electron. Struct. **2**, 034001 (2020).
- [50] M. Calderón and E. Bascones, Phys. Rev. B **102**, 155149 (2020).
- [51] M. Xie and A. H. MacDonald, Phys. Rev. Lett. **124**, 097601 (2020).
- [52] N. Bultinck, E. Khalaf, S. Liu, S. Chatterjee, A. Vishwanath, and M. P. Zaletel, Phys. Rev. X **10**, 031034 (2020).
- [53] S. Liu, E. Khalaf, J. Y. Lee, and A. Vishwanath, arXiv:1905.07409 (2019).
- [54] Y. Zhang, K. Jiang, Z. Wang, and F. Zhang, Phys. Rev. B **102**, 035136 (2020).
- [55] T. Cea and F. Guinea, Phys. Rev. B **102**, 045107 (2020).
- [56] J. González and T. Stauber, Phys. Rev. B **102**, 081118(R) (2020).
- [57] A. O. Sboychakov, A. V. Rozhkov, A. L. Rakhmanov, , and F. Nori, Phys. Rev. B **100**, 045111 (2019).
- [58] T. C. O’Connor, J. Andzelm, and M. O. Robbins, J. Chem. Phys. **142**, 024903 (2015).
- [59] A. N. Kolmogorov and V. H. Crespi, Phys. Rev. B **71**, 235415 (2005).
- [60] S. Plimpton, J. Comp. Phys. **117**, 1 (1995).
- [61] J. C. Slater and G. F. Koster, Phys. Rev. **94**, 1498 (1954).
- [62] P. Moon and M. Koshino, Phys. Rev. B **85**, 195458 (2012).
- [63] J. M. Pizarro, M. Rosner, R. Thomale, R. Valent, and T. O. Wehling, Phys. Rev. B **100**, 161102(R) (2019).
- [64] Z. A. H. Goodwin, F. Corsetti, A. A. Mostofi, and J. Lischner, Phys. Rev. B **100**, 235424 (2019).
- [65] Z. A. H. Goodwin, V. Vitale, F. Corsetti, D. Efetov, A. A. Mostofi, and J. Lischner, Phys. Rev. B **101**, 165110 (2020).
- [66] H. Q. Lin and J. E. Hirsch, Phys. Rev. B **35**, 3359 (1987).
- [67] T. O. Wehling, E. Şaşıoğlu, C. Friedrich, A. I. Lichtenstein, M. I. Katsnelson, and S. Blügel, Phys. Rev. Lett. **106**, 236805 (2011).
- [68] M. Schüler, M. Rösner, T. O. Wehling, A. I. Lichtenstein, and M. I. Katsnelson, Phys. Rev. Lett. **111**, 036601 (2013).
- [69] A. Fischer, L. Klebl, C. Honerkamp, and D. M. Kennes, Spin-fluctuation-induced pairing in twisted bilayer graphene (2020), arXiv:2008.12532 [cond-mat.suprcon].